J Appl Electrochem (2014) 44:1153–1163
DOI 10.1007/s10800-014-0717-8

RESEARCH ARTICLE

$LiFePO_4$ batteries with enhanced lithium-ion-diffusion ability due to graphene addition

Van Hiep Nguyen · Hal-Bon Gu

Received: 30 April 2014 / Accepted: 14 July 2014 / Published online: 17 August 2014

Abstract In this study, graphene was added to $LiFePO_4$ via a hydrothermal method to improve the lithium-ion-diffusion ability of $LiFePO_4$. The influence of graphene addition on $LiFePO_4$ was studied by X-ray diffraction (XRD), field emission scanning electron microscopy, transmission electron microscopy, cyclic voltammetry, cycling test, and AC impedance analysis. The addition of graphene to $LiFePO_4$ resulted in the formation of a $LiFePO_4$–graphene composite; XRD observations revealed the composite to have a single phase with an olivine-type structure. Furthermore, $LiFePO_4$ particles in the composite were stacked on the graphene sheet surface, thereby enabling the composite to form an effective conducting network and facilitate the penetration of the surface of active materials by an electrolyte. The lithium-ion-diffusion ability of the $LiFePO_4$–graphene composite was greater than that of pure $LiFePO_4$. Of a number of materials studied [namely, pure $LiFePO_4$, $LiFePO_4$–graphene (1 %), $LiFePO_4$–graphene (5 %), and $LiFePO_4$–graphene (8 %)], $LiFePO_4$–graphene (5 %) delivered the best electrochemical performance with a lithium-ion-diffusion coefficient of 8.18×10^{-12} cm^2 s^{-1} and the highest specific discharge capacity of 149 mAh g^{-1} at 0.17 C; in contrast, the corresponding values for pure $LiFePO_4$ were 3.01×10^{-12} cm^2 s^{-1} and 109 mAh g^{-1}, respectively. Further, $LiFePO_4$–graphene (5 %) showed a very high specific discharge capacity of 170 mAh g^{-1} at 0.1 C, which is equal to the theoretical capacity of $LiFePO_4$.

Keywords Lithium-ion-diffusion coefficient · Impedance · Hydrothermal method · Graphene

V. H. Nguyen · H.-B. Gu (✉)
Department of Electrical Engineering, Chonnam National University, Gwangju 500-757, South Korea
e-mail: hbgu@chonnam.ac.kr

1 Introduction

Nowadays, the demand for portable electrical equipment has grown considerably. Rechargeable lithium-ion batteries with no memory effect and slow loss of charge when not in use are required in many applications. Lithium-ion batteries can be used in many devices such as notebooks, computers, cameras, hybrid electric vehicles, and portable electronic devices. In these lithium-ion batteries, the cathode plays an important role in determining the capacity and ability of the batteries. Many materials have been used to fabricate cathodes for lithium-ion batteries, such as $LiCoO_2$, $LiNiO_2$, $LiFePO_4$, and $LiMn_2O_4$. Of these materials, $LiFePO_4$ is currently being researched extensively, owing to its high theoretical specific capacity ($\sim$170 mAh g^{-1}), low cost, high safety, and high compatibility with the environment [1–3]. Unfortunately, one drawback of $LiFePO_4$ that has still not been addressed is its low electronic conductivity, which makes it difficult for $LiFePO_4$ to attain its full capacity. Poor rate capability and low lithium-ion diffusion in the battery structure are other issues that remain to be solved. Many efforts have been made to overcome these drawbacks. These efforts involve the following three main methods: adding conductive additives including a carbon source [4, 5]; doping $LiFePO_4$ with isovalent, supervalent, and subvalent ions such as Zn^{2+}, Si^{2+}, Mn^{2+}, Al^{3+}, and Ti^{4+} [6–10]; and controlling the properties of $LiFePO_4$ particles, such as texture, size, and morphology [11].

For obtaining a cathode material with improved electrochemical properties that could be used in lithium-ion batteries, our research group studied a $LiFePO_4$–graphite nanofiber composite [12]. Nanotube-like graphite nanofibers are not easily obtainable, and their structure cannot be controlled. Further, the resultant particle size and

connection between $LiFePO_4$ particles in the $LiFePO_4$–graphite composite are not as good as desired. Thus, the cycling stability and discharge capacity of these composites are too poor to be compared to those of $LiFePO_4$ reported in many previous papers. In order to improve these properties, graphene was utilized. Graphene has a sheet-like form, owing to which it can form an effective conducting network as well as facilitate the penetration of the surface of active materials by an electrolyte. Furthermore, owing to its excellent properties such as high electronic conductivity, structural flexibility, stability, and mechanical strength, graphene has found a variety of applications in energy conversion, storage devices, and $LiFePO_4$ battery [13–16]. To date, several methods have been employed to prepare $LiFePO_4$–graphene composites. Wang et al. [17] reported $LiFePO_4$/graphene composites prepared through a hydrothermal route followed by heat-treatment with graphite oxide used as precursor material. Wang et al. [18] synthesized $LiFePO_4$/graphene composites with excellent electrochemical properties by solid-state method. A graphene-encapsulated $LiFePO_4$ composite has been synthesized by Lou et al. [16], using self-assembly of surface-modified $LiFePO_4$; Kim et al. [19] synthesized graphene-embedded $LiFePO_4$ using a catalyst-assisted self-assembly method with superior cycling performance and rate capability; and a composite was also prepared by Ding et al. [20], using co- precipitation method. However, these preparation approaches are complicated. Thus, in this study, graphene was added to $LiFePO_4$, forming a $LiFePO_4$-graphene composite, by a facile hydrothermal method to improve the electrochemical properties of $LiFePO_4$. It is expected that graphene not only played the role of a conductive material improving the electrochemical properties of $LiFePO_4$ but also acted as a separator preventing the growth of $LiFePO_4$ particles. Furthermore, in the papers mentioned above, owing to the improved lithium-ion-diffusion ability of the composite, the electrochemical and cycling performances of the battery increased considerably. However, the detailed measurement about the increase of lithium-ion-diffusion ability was not carried out. Therefore, in this paper, the lithium-ion-diffusion ability was considered and evaluated.

2 Experimental

First, $LiFePO_4$ was synthesized using the following precursor materials: $LiOH{\cdot}H_2O$ (Aldrich Co., purity: 99.95 %), $FeSO_4{\cdot}7H_2O$ (Aldrich Co., purity: >99 %), H_3PO_4 (Aldrich Co., purity: >99.999 %), and $C_6H_8O_6$ (Aldrich Co., purity: >99 %). All materials were mixed in respective stoichiometric amounts and stirred for 1 h until a white-green homogenous mixture was obtained. The mixture was transferred to a Teflon-lined autoclave, heated at 170 C for 12 h, and subsequently cooled down to room temperature. The obtained solution was filtered and washed many times with distilled water. The obtained $LiFePO_4$ powder was milled with different amounts (wt%) of graphene (thickness: 6–8 nm, purity: 99.5 %, surface area: 120–150 $m^2\ g^{-1}$; Enanotech Co.) by a planetary mono mill (Pulverisette 6, Fritsch, Germany). The obtained powder was dried at 90 °C for 12 h and pelleted, and then subsequently annealed at 500 °C for 1 h under nitrogen gas in a tubular oven (J-FCA, Jisico, Korea). After ball-milling and drying, $LiFePO_4$–graphene powder was obtained. This process is illustrated in Fig. 1.

For evaluating the electrochemical properties of the obtained composite, $LiFePO_4$–graphene composite electrodes were fabricated using the as-prepared cathode materials, SP-270, and polyvinylidene fluoride (PVDF) with a weight ratio of 70:25:5 in *N*-methylpyrrolidone (NMP). The obtained slurry was coated onto an Al foil, dried at 90 °C for 1 h, and was then roll-pressed. The electrodes were then dried again at 110 °C for 24 h under vacuum prior to use. Cells were assembled using lithium metal as the anode and 1 M $LiPF_6$/EC-DMC (1:1) as the electrolyte in an argon-filled glove box.

The crystallite phase of the synthesized $LiFePO_4$–graphene composite was identified using high-resolution X-ray diffraction (HR-XRD, D/MAX Ultima III, Rigaku, Japan) with scanning steps of 0.02° over the range 10°–50°. The morphology of the $LiFePO_4$–graphene composite was observed by field emission scanning electron microscopy (FE-SEM, Hitachi, Japan) and transmission electron microscopy (TEM, JEOL JFE-2000 FXII, Japan).

Cyclic voltammetry (CV) was performed at a scanning rate of 0.1 mV s^{-1} in the voltage range 2.3–4.5 V. The charge–discharge cycle performance of the cells was evaluated using a galvanostatic charge–discharge unit battery cycler (WBCS-3000, WonATech, Korea) in the voltage range 2.5–4.0 V at various discharge C-rates ranging from 0.1 to 5 C at 25 °C. Electrochemical impedance spectroscopy (EIS) was potentiostatically carried out using an impedance system (ZAHNER IM6, Germany) by applying an AC voltage with an amplitude of 5 mV over the frequency range 2 MHz–10 mHz.

3 Results and discussion

The XRD patterns of $LiFePO_4$–graphene powder are shown in Fig. 2. All the patterns could be indexed to a single-phase material having an orthorhombic structure with the space group Pnma [21]. This proves that the addition of graphene had no effect on the structure of $LiFePO_4$. Further, no (002) diffraction peak of graphite

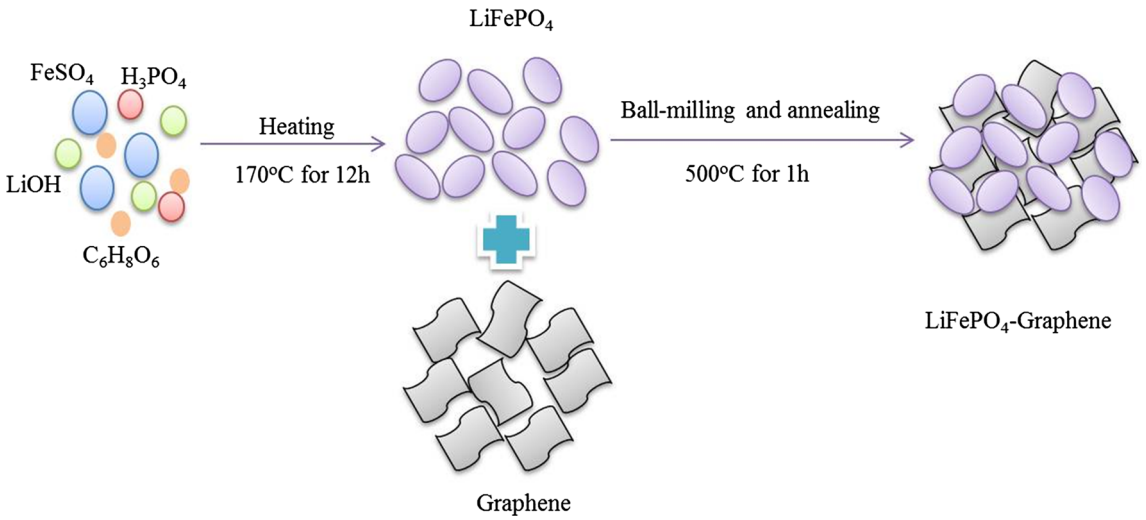

Fig. 1 Schematic illustration of $LiFePO_4$–graphene composite preparation

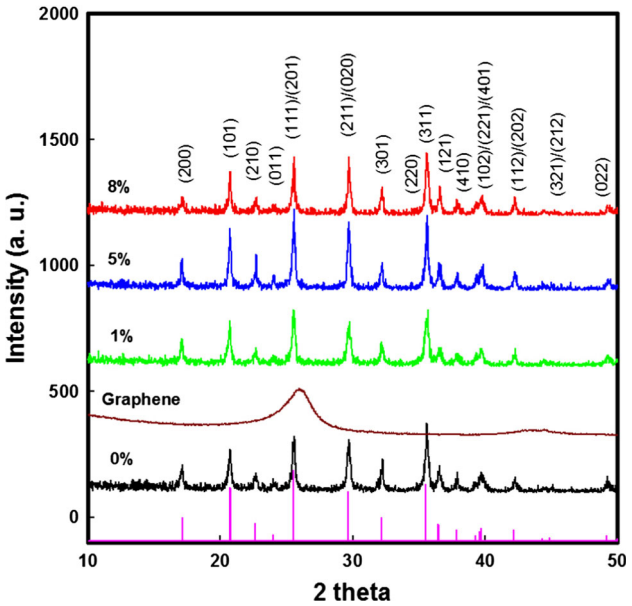

Fig. 2 XRD patterns for $LiFePO_4$–graphene composites

located around 26.5° was observed (Fig. 2). Furthermore, the unit cell parameters of $LiFePO_4$–graphene were calculated, and they are listed in Table 1. As shown in this table, graphene addition resulted in a slight reduction in the unit cell parameters of $LiFePO_4$. This can be explained by graphene suppressing the growth size of $LiFePO_4$ in the annealing process. This effect also appeared in the case of other carbon sources in our early research on PSS and PSS/MWCNT [22–24]. $LiFePO_4$–graphene exhibited the smallest volume of 290.4017 $Å^3$. Moreover, the crystallite size (L) of the sample was calculated from raw data obtained via XRD analysis by using Scherrer's equation [25]:

$$L = \frac{0.89\lambda}{\beta \cos\theta}, \tag{1}$$

where β is the full-width at half maximum, and λ is the X-ray wavelength (1.54056 Å). The results show that the crystallite size decreased upon graphene addition. The crystallite sizes for $LiFePO_4$, $LiFePO_4$–graphene (1 %), $LiFePO_4$–graphene (5 %), and $LiFePO_4$–graphene (8 %) were 66, 59, 45, and 57 nm, respectively. The crystallite size tended to decrease, which plays an important role in determining the intercalation/deintercalation capability of lithium ions in the bulk of cathode materials, leading to an increase in the lithium-ion-diffusion ability of $LiFePO_4$ [15].

In addition to the intensity variation, the crystallization of particles for various orientations and morphologies was calculated from Fig. 2. The percentage of $LiFePO_4$–graphene crystals in different orientations (*hkl*) was estimated as below:

$$\%hkl = \frac{I_{hkl}/I^*_{hkl}}{\sum\left(I_{hkl}/I^*_{hkl}\right)} \tag{2}$$

where I_{hkl} is the measured diffraction intensity of XRD peaks for $LiFePO_4$–graphene (1 %), $LiFePO_4$–graphene (5 %), and $LiFePO_4$–graphene (8 %); and I^*_{hkl} is the diffraction intensity of the XRD profile for $LiFePO_4$ powder [12, 26, 27]. The calculation results are listed in Table 2. It can be clearly observed that the percentages of (210) orientations for the $LiFePO_4$–graphene (5 %) are larger than those for $LiFePO_4$ powder, indicating that (210) nucleation planes were predominant in $LiFePO_4$ powder.

Table 1 Unit cell parameters for $LiFePO_4$–graphene

wt%	a (Å)	b (Å)	c (Å)	V (Å^3)	$\alpha = \beta = \gamma$	Crystallite size (nm)
0	10.3494	6.0359	4.6999	293.5949	90°	66
1	10.3648	5.9962	4.7089	292.3578	90°	59
5	10.3536	5.9576	4.7035	290.4017	90°	45
8	10.3534	5.9839	4.7044	291.4556	90°	57

Table 2 Crystallographic orientation of $LiFePO_4$–graphene composites

hkl	Standard intensity	*%hkl* (1 %)	*%hkl* (5 %)	*%hkl* (8 %)
200	92	8.31	7.40	5.25
101	150	9.72	9.74	9.08
210	61	8.68	12.79	7.49
011	211	8.39	9.08	8.95
201	194	7.34	8.43	9.78
211	122	5.98	5.07	7.35
301	254	6.80	6.88	7.57
311	97	5.64	6.37	9.42
121	69	5.03	5.79	6.75
410	70	7.57	7.94	8.62
401	52	10.85	8.16	10.44
202	20	9.55	7.80	4.74
022	51	6.13	4.53	4.56

The surface morphologies of the $LiFePO_4$–graphene composites were observed by FE-SEM and TEM (Fig. 3). As shown in Fig. 3c, d, graphene provided a transport infrastructure path between $LiFePO_4$ particles. The existence of graphene can be seen more clearly with the $LiFePO_4$ particles stacked on the graphene surface. Graphene, likely formed as sheets, can form an effective conducting network and facilitate the penetration of the surface of active materials by an electrolyte. Further, graphene enhances the connection availability between $LiFePO_4$ particles as well. Thus, lithium ions in the $LiFePO_4$–graphene composite could diffuse between the $LiFePO_4$ particles more easily, which resulted in superior rate capability and higher reversible capacities in comparison with $LiFePO_4$ particles.

A comparison of the cyclic voltammograms of pure $LiFePO_4$ and $LiFePO_4$–graphene composite at 0.1 mV s^{-1} is shown in Fig. 4a. A pair of redox peaks is clearly observed in every curve, indicating only one well-defined step in the electrochemical process of oxidation–reduction for $LiFePO_4$. The major differences between pure $LiFePO_4$ and the $LiFePO_4$–graphene composite are in their peak currents (I_P) and redox peak potentials (E_p). As shown in Fig. 4a, the peak intensity of $LiFePO_4$–graphene (5 %) is about two times that of pure $LiFePO_4$ (1.06 mA for $LiFePO_4$–graphene (5 %) and 0.5 mA for pure $LiFePO_4$). Moreover, the difference in the peak potentials is much smaller for $LiFePO_4$–graphene than that for pure $LiFePO_4$, except for a slight low peak current for $LiFePO_4$–graphene (1 %). It was confirmed that the $LiFePO_4$–graphene composite showed faster lithium-ion diffusion than pure $LiFePO_4$. To investigate in detail the effects of graphene addition to $LiFePO_4$, the lithium-ion diffusion coefficient attributed to the kinetic and thermodynamic properties of the electrodes was determined by CV. The reversibility of pure $LiFePO_4$ and the $LiFePO_4$–graphene composite was studied by varying the scan rate between 0.01 and 1 mV s^{-1} (Fig. 4b–e).

As shown in Fig. 4b–e, the higher the scanning rate is, the higher and larger the redox peaks are. That is because the peak area divided by the scanning rate yields the capacity of the electrode, which should be a constant [28]. The reduction peaks shift to the left (low potential), and the oxidation peaks shift to the right (high potential) with the increasing scanning rate. Further, the I_p increases while scanning rate increases. Notably, the oxidation peaks are slightly higher than the reduction peaks, indicating a slight kinetic difference between lithium insertion and extraction processes, especially at the scanning rate of 1 mV s^{-1}. This is because of the disparities in the insertion and extraction capacities of lithium ions into the electrode at a high scanning rate, which causes irreversible behaviors.

Typically, the interpretation of CV results for the $LiFePO_4$ system has still been controversial. According to Franger et al. [29], the $LiFePO_4$ system is almost irreversible and rapid because of the linear relationship between I_p and the scanning rate (v), whereas others suggested that it is reversible [30–32]. He et al. [27] and Kanoh et al. [33] suggested that the lithium-ion insertion/extraction for $LiFePO_4$ can be considered an irreversible system. Thus, a linear relationship between I_p and the scanning rate ($v^{1/2}$) was detected as well. Consequently, CV data were analyzed on the basis of an electrochemically irreversible system. The reaction of the electrode materials was not in equilibrium, indicating that the forward and reverse reaction rates had a wide disparity and the ionic transports across particle boundaries were not similar. Using the data obtained from CV curves, the apparent diffusion coefficients (D_{Li}) of $LiFePO_4$–graphene are estimated [27, 29, 34–36].

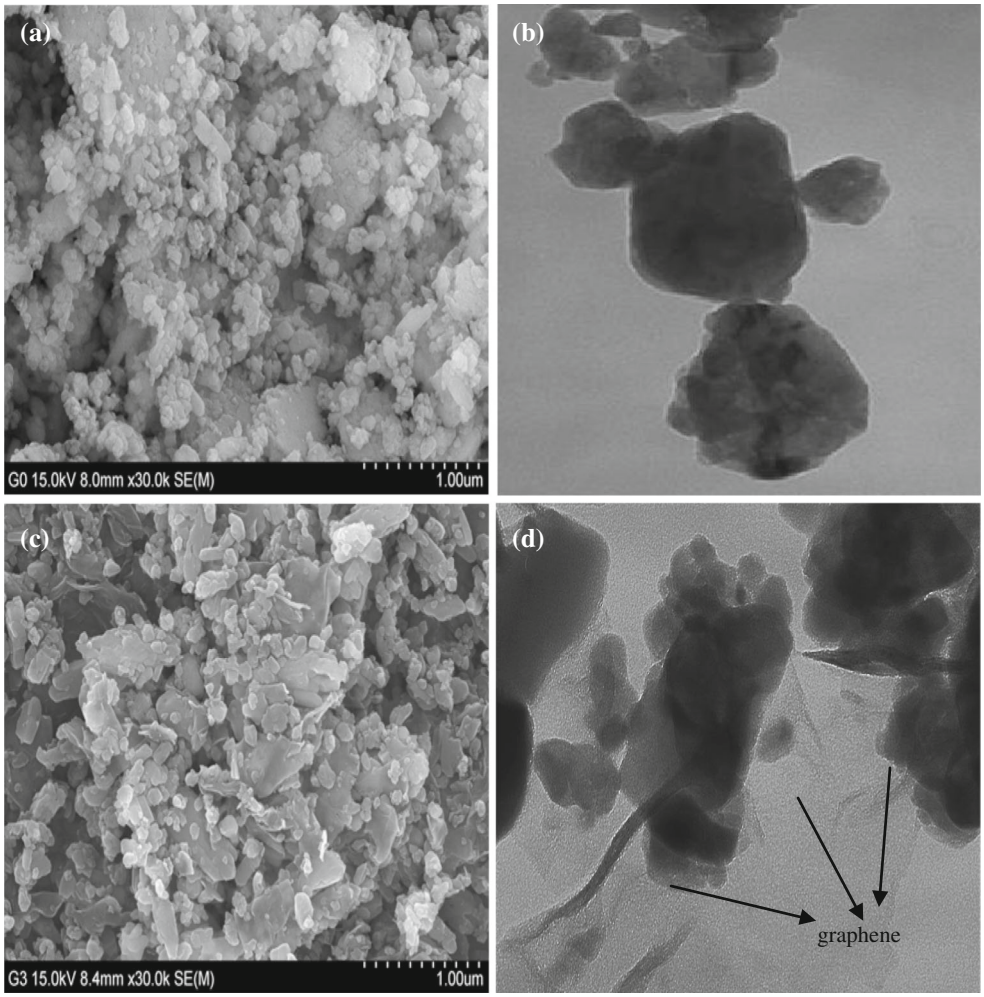

Fig. 3 SEM and TEM images of **a**, **b** $LiFePO_4$ and **c**, **d** $LiFePO_4$–graphene

$$i_p = (2.69 \times 10^5)(\alpha n)^{1/2} A \Delta C_{Li} D_{Li}^{1/2} v^{1/2} \quad (3)$$

$$/E_p - E^\circ/ = \left(\frac{RT}{\alpha nF}\right)\left\{0.78 + \ln\left(\frac{D_{Li}^{1/2}}{k^\circ}\right) + \ln\left(\frac{\alpha nFv}{RT}\right)^{1/2}\right\} \quad (4)$$

where I_p is the peak current, n is the number of electrons per lithium ion ($n = 1$), v is the scanning rate of cyclic voltammetry, ΔC_{Li} is the concentration of lithium ions, A is the actual surface area of the electrode, $/E_p - E^0/$ is calculated as half of the difference between redox peak potentials, α is the transfer coefficient, and k^0 is the standard rate constant. The plots of $/E_p - E^0/$ vs. lnv and I_p vs. $v^{1/2}$ are illustrated in Fig. 5a, b. The transfer coefficient (α) is obtained from Fig. 5a and Eq. 4. The values of D_{Li} for pure $LiFePO_4$ and $LiFePO_4$–graphene can be obtained from Fig. 5b if the obtained value of α is known. The peak current (I_p) exhibits a linear relation with the square root of the scanning rate ($v^{1/2}$), as shown in Fig. 5b. This is a typical diffusion-controlling response. It indicates that the kinetics of the two-phase transition in $LiFePO_4$ behaves similarly to a diffusion process. Further, it was found that $LiFePO_4$ displays an apparent diffusion coefficient lower than that of $LiFePO_4$–graphene in the extraction process; this confirms that the extraction of lithium ions in $LiFePO_4$–graphene is better than that in pure $LiFePO_4$. The calculated values of the apparent diffusion coefficient of pure $LiFePO_4$, $LiFePO_4$–graphene (1 %), $LiFePO_4$–graphene (5 %), and $LiFePO_4$–graphene (8 %) are 3.01×10^{-12}, 3.99×10^{-12}, 8.18×10^{-12}, and 5.21×10^{-12} $cm^2\ s^{-1}$, respectively. The difference in D_{Li} for the $LiFePO_4$–graphene composite is due to a different interfacial charge-transfer mechanism, which is an important factor in lithium-ion diffusion, leading to a different rate performance.

The EIS results for $LiFePO_4$–graphene after 3 cycles are shown in Fig. 6. The semicircles at high to medium frequency are mainly related to a complex reaction process at

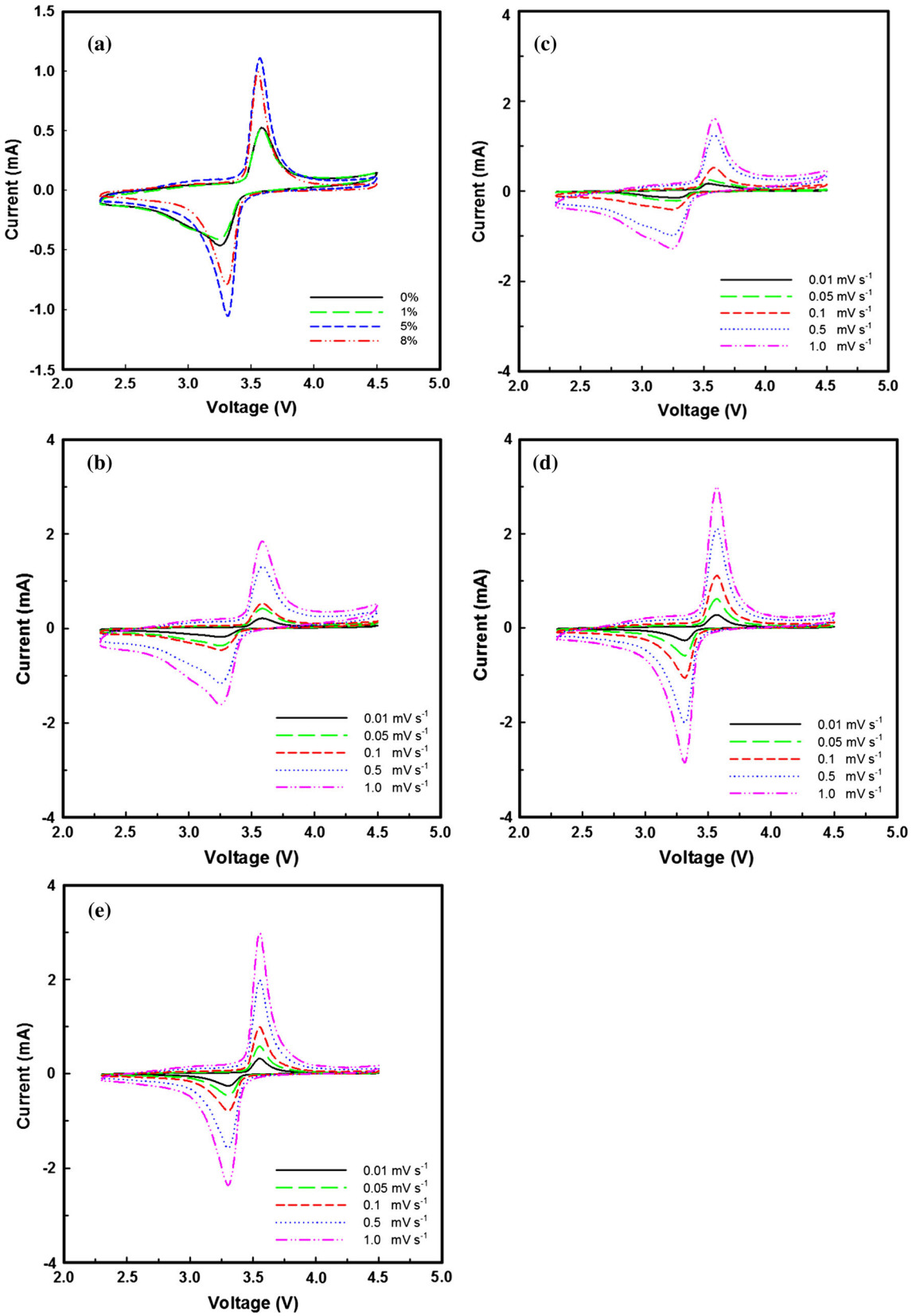

Fig. 4 Cyclic voltammetry profiles for **a** $LiFePO_4$–graphene at a scan rate of 0.1 mV s^{-1}, and **b** $LiFePO_4$, **c** $LiFePO_4$–graphene (1 %), **d** $LiFePO_4$–graphene (5 %), and **e** $LiFePO_4$–graphene (8 %) at various scan rates

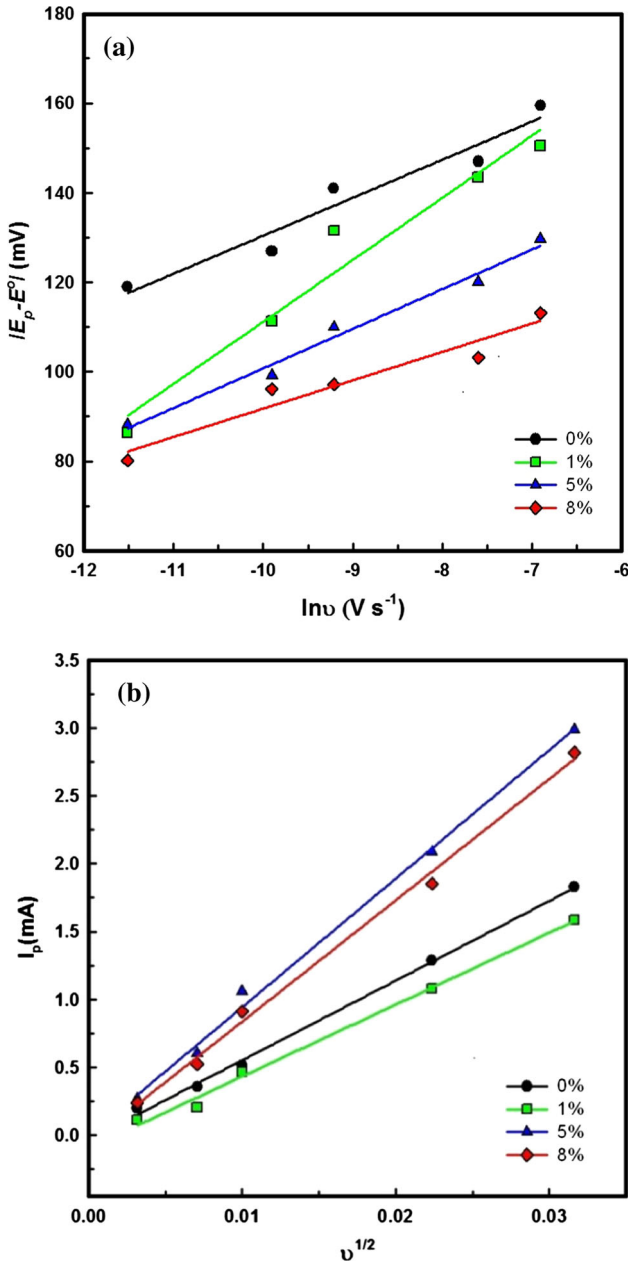

Fig. 5 Graphs for $LiFePO_4$ and $LiFePO_4$–graphene showing the relationship between **a** $|E_p - E^0|$ and lnv, **b** I_p and $v^{1/2}$

the electrolyte/cathode interface. The inclined line in the lower frequency region is attributed to the Warburg impedance, which is associated with lithium-ion diffusion in the $LiFePO_4$ electrode [36]. The impedance spectra fitted using an equivalent circuit in which Z_w is the Warburg impedance, R_{ct} is the charge-transfer resistance, C_d is the capacitance of a double layer, and R_s is the ohmic resistance as indicated in Fig. 6. The exchange current density is calculated using the following equation:

$$i^0 = \frac{RT}{nFR_{ct}}. \quad (5)$$

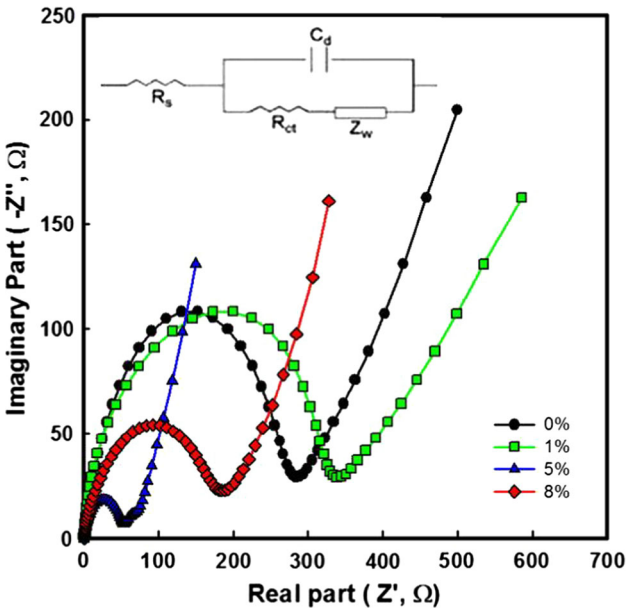

Fig. 6 EIS results for $LiFePO_4$–graphene after 3 cycles

Table 3 Impedance parameters for the cells prepared from $LiFePO_4$–graphene composites

wt%	R_s (Ω)	R_{ct} (Ω)	i^o (mA cm^{-2})
0	0.60	283	9.07×10^{-5}
1	0.65	338	7.59×10^{-5}
5	0.50	50	5.14×10^{-4}
8	0.60	180	1.43×10^{-4}

It can be observed that the diameter of the high-frequency-combined semicircle decreases with enhancement in the quantities pertaining to graphene. Impedance parameters of the batteries prepared from $LiFePO_4$–graphene composites are shown in Table 3. In the results, the R_s values for pure $LiFePO_4$ and the $LiFePO_4$–graphene composite are similar. It can also be seen that the charge-transfer resistance of the $LiFePO_4$–graphene composite is smaller than that of pure $LiFePO_4$; further, the exchange current density increases with enhancement in the quantities pertaining to graphene, especially for $LiFePO_4$–graphene (5 %). Since the $LiFePO_4$–graphene composite shows the lowest resistance and the largest exchange current density, it is suggested that graphene addition to the $LiFePO_4$ particle surface significantly improved the performance of the Li battery in accordance with the CV results.

Figure 7 illustrates the cycling performance and coulombic eficiency of $LiFePO_4$–graphene charged–discharged at 0.17 C in the voltage range 2.5–4.0 V. The discharge capacities of $LiFePO_4$ that appeared at the 2nd and 30th cycles are 109 and 93 mAh g^{-1}, respectively. After graphene addition, the discharge capacity of the

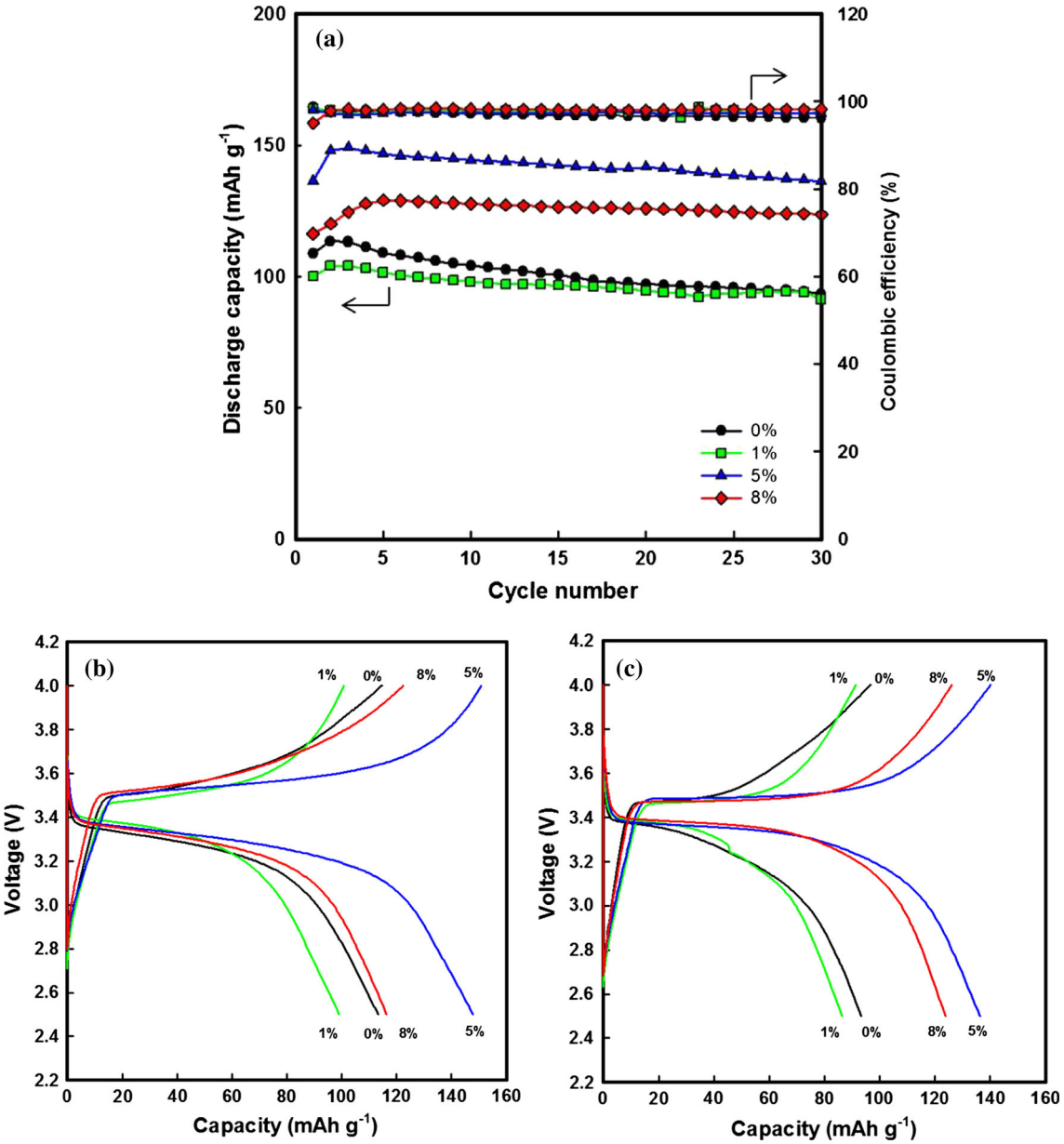

Fig. 7 **a** Cycling performance and coulombic efficiency of $LiFePO_4$–graphene, and charge–discharge curves of $LiFePO_4$–graphene **b** at the 2nd cycle, **c** at the 30th cycle

battery increases. Taking into account the results suggested by XRD patterns, SEM, TEM, CV, and the apparent lithium-ion diffusion, we can deduce that the intercalation/deintercalation of lithium ions into the active material in the $LiFePO_4$–graphene electrode occurs more easily during the charging–discharging process. Indeed, the $LiFePO_4$–graphene (5 %) delivered the highest discharge capacity of 136 mAh g^{-1} at the initial cycle and after 30 cycles, and the best value of 149 mAh g^{-1} was observed at the third cycle. The coulombic efficiency of $LiFePO_4$–graphene still maintains at 97–100 % for all samples. Moreover, the polarization between the charge and discharge plateaus of $LiFePO_4$–graphene electrode was less than that of another sample, also illustrating that the kinetics of Li^+ diffusion was improved by graphene addition (Fig. 7b, c). In comparison with $LiFePO_4$, the best discharge capacity of $LiFePO_4$–graphene (5 %) was higher by 46 %. Therefore, 5 % was considered as the optimum concentration for the $LiFePO_4$–graphene composite in this study.

The discharge curves of $LiFePO_4$ and $LiFePO_4$–graphene (5 %) at various scanning rates are shown in Fig. 8. The discharge capacity of $LiFePO_4$–graphene (5 %) varies in the range 170–98 mAh g^{-1} at the rate of 0.1–5 C (123–28 mAh g^{-1} for $LiFePO_4$). The capacity of this

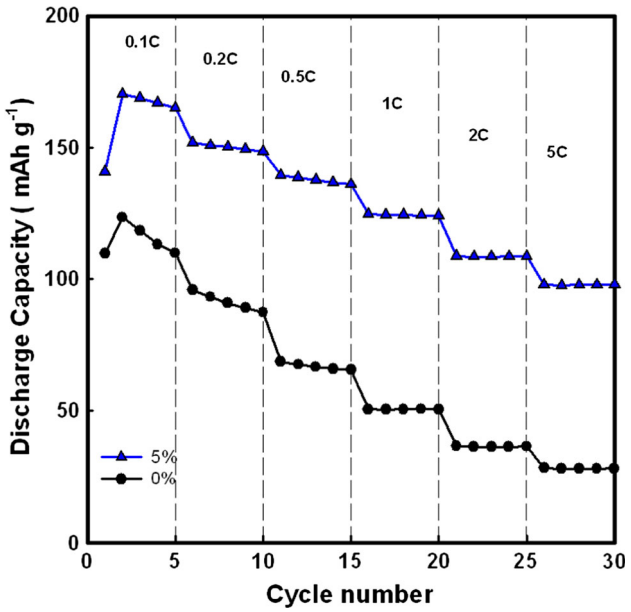

Fig. 8 Discharge curves for $LiFePO_4$ and $LiFePO_4$–graphene (5 %) at different scan rates

material at a low rate is equal to the theoretical value for a $LiFePO_4$ battery and its high retention of rate capability. The highly stable reversible capacity of 98 mAh g^{-1} is obtained at the highest current density of 5 C, while this value is only 28 mAh g^{-1} for $LiFePO_4$. The results show that there is difference between the capacities of $LiFePO_4$–graphene (5 %) at scan rates in the range 0.1–5C, which indicates that other factors such as the interface, polarization, and connection also depend on the capacity of the $LiFePO_4$ battery [37, 38]. Moreover, the rate capability and cycling performance of $LiFePO_4$–graphene in this paper are higher than the $LiFePO_4$–graphene reported in previous work, which was synthesized by hydrothermal method [17], but lower than when compared with the related reports that exist in the literature. That is because in the other works, $LiFePO_4$ or graphene was optimized about morphology. And more detailed comparisons can be found in Table 4. We believe that if particle size of $LiFePO_4$ and graphene are optimized well, discharge capacity and cycling stability of $LiFePO_4$ will get better.

4 Conclusions

$LiFePO_4$–graphene composites were synthesized successfully by the hydrothermal method. To improve the lithium-ion-diffusion ability of $LiFePO_4$, different amounts of graphene were added to $LiFePO_4$. The XRD results demonstrated that $LiFePO_4$–graphene composites had an orthorhombic olivine-type structure with a Pnma space group and the smallest volume of 290.4017 $Å^3$. The percentages of (210) orientations in $LiFePO_4$–graphene (5 %) were clearly larger than those in the $LiFePO_4$ powder, indicating the predominant presence of (210) nucleation planes. According to FE-SEM and TEM images, graphene likely formed sheets that formed an effective conducting network and facilitated the penetration of the surface of active materials by the electrolyte, as well as prevented the aggregation of $LiFePO_4$ particles. CV results indicated that the kinetics of the two-phase transition in $LiFePO_4$ behaves similarly to a diffusion process. Further, it was found that $LiFePO_4$ displays an apparent diffusion coefficient lower than that of $LiFePO_4$–graphene in the extraction process; this confirmed that the extraction of lithium ions in $LiFePO_4$–graphene is better than that in pure $LiFePO_4$. $LiFePO_4$–graphene (5 %) delivered the fastest lithium-ion diffusion with a lithium-ion-diffusion coefficient of 8.18×10^{-12} cm^2 s^{-1}; moreover, it showed the highest specific discharge capacities of 149 mAh g^{-1} at 0.17 C (whereas it was 109 mAh g^{-1} for pure $LiFePO_4$) and 170 mAh g^{-1} at 0.1 C.

Table 4 The electrochemical properties of $LiFePO_4$–graphene synthesized by different methods

Synthetic processes	Electrochemical performance	References
Co-precipitation method	160 mA h g^{-1} at 0.2 C, 145 mAh g^{-1} at 1 C and 120 mAh g^{-1} at 5 C	[20]
Catalyst assisted self-assembly method	152 mAh g^{-1} at 0.1 C and 140 mAh g^{-1} at 1 C	[19]
Solid state method	160 mAh g^{-1} at 0.1 C, 140 mAh g^{-1} at 1 C and 125 mAh g^{-1} at 5 C	[18]
Self-assembly method	118 mAh g^{-1} at 1 C, 100 mAh g^{-1} at 5 C and 80 mAh g^{-1} at 50 C	[16]
Hydrothermal method with graphite oxide used as precursor material	160 mAh g^{-1} at 0.1 C, 123 mAh g^{-1} at 1 C and 90 mAh g^{-1} at 5 C	[17]
Hydrothermal method	170 mAh g^{-1} at 0.1 C, 125 mAh g^{-1} at 1 C and 98 mAh g^{-1} at 5 C	Current study

References

1. Padhi AK, Nanjundaswamy KS, Goodenough JB (1997) Phospho-olivines as positive-electrode materials for rechargeable lithium batteries. J Electrochem Soc 11:188–1194. doi:10.1149/1.1837571
2. Wang WL, Nguyen VH, Jin EM, Gu HB (2013) Si–SnO composite as an anode material in lithium ion batteries using novel polymer binder. Mater Express 3:273–279. doi:10.1166/mex.2013.1124
3. Gu HB, Jun DK, Park GC, Jin B, Jin EM (2007) Nanosized $LiFePO_4$ cathode materials for lithium ion batteries. J Nanosci Nanotechnol 7:3980–3984. doi:10.1166/jnn.2007.079
4. Bard AJ, Faulkner LR (2001) Electrochemical Methods, 2nd edn. Wiley, New York
5. Jin EM, Jin B, Jun DK, Park KH, Gu HB, Kim KW (2008) A study on the electrochemical characteristics of $LiFePO_4$ cathode for lithium polymer batteries by hydrothermal method. J Power Sources 178:801–806. doi:10.1016/j.jpowsour
6. Shenouda AY, Liu HK (2009) Studies on electrochemical behaviour of zinc-doped $LiFePO_4$ for lithium battery positive electrode. J Alloy Compd 477:498–503. doi:10.1016/j.jallcom.2008.10.077
7. Amin R, Lin C, Peng J, Weichert K, Acartürk T, Starke U, Maier J (2009) Silicon-doped $LiFePO_4$ single crystals: growth, conductivity behaviour and diffusivity. Adv Funct Mater 19:1697–1704. doi:10.1002/adfm.200801604
8. Abbate M, Lala SM, Montoro LA, Rosolenb JM (2005) Ti-, Al-, and Cu-doping induced gap states in $LiFePO_4$. Electrochem Solid-State Lett 8:A288–A290. doi:10.1149/1.1895286
9. Prosini PP, Zane D, Pasquali M (2001) Improved electrochemical performance of a $LiFePO_4$-based composite cathode. Electrochim Acta 46:3517–3523. doi:10.1016/s0013-4686(01)00631-4
10. Li H, Wang ZX, Chen LQ, Huang XJ (2009) Research on advanced materials for Li-ion batteries. Adv Mater 21:4593–4607. doi:10.1002/adma.200901710
11. Yamada A, Chung SC, Hinikuma K (2001) Optimized $LiFePO_4$ for lithium battery cathodes. J Electrochem Soc 148:A224–A229. doi:10.1149/1.1348257
12. Nguyen VH, Jin EM, Gu HB (2013) Synthesis and electrochemical properties of $LiFePO_4$-graphite nanofiber composites as cathode materials for lithium ion batteries. J Power Sources 244:586–591. doi:10.1016/j.jpowsour.2013.01.073
13. Hu LH, Wu FY, Lin CT, N.K A, Li LJ (2013) Graphene-modified $LiFePO_4$ cathode for lithium ion battery beyond theoretical capacity. Nat Commun 4:1687. doi:10.1038/ncomms2705
14. Yang J, Wang J, Tang Y, Wang D, Li X, Hu Y, Li R, Liang G, Sham TK, Sun X (2013) $LiFePO_4$–graphene as a superior cathode material for rechargeable lithium batteries: impact of stacked graphene and unfolded graphene. Energy Environ Sci 6:1521–1528. doi:10.1039/c3ee24163g
15. Liu T, Zhao L, Zhu J, Wang B, Guo C, Wang D (2014) The composite electrode of $LiFePO_4$ cathode materials modified with exfoliated graphene from expanded graphite for high power Li-ion batteries. J Mater Chem A 2:2822–2829. doi:10.1039/c3ta14713d
16. Luo WB, Chou SL, Zhai YC, Liu HK (2014) Self-assembled graphene and $LiFePO_4$ composites with superior high rate capability for lithium ion batteries. J Mater Chem A 2:4927–4931. doi:10.1039/c3ta14471b
17. Wang L, Wang HB, Liu ZH, Xiao C, Dong SM, Han PX, Zhang ZY, Zhang XY, Bi CF, Cui GL (2010) A facile method of preparing mixed conducting $LiFePO_4$/graphene composites for lithium-ion batteries. Solid State Ionics 181:1685–1689. doi:10.1016/j.ssi.2010.09.056
18. Wang Y, Feng ZS, Chen JJ, Zhang C (2012) Synthesis and electrochemical performance of $LiFePO_4$/graphene composites by solid-state reaction. Mate Lett 71:54–56. doi:10.1016/j.jpowsour.2012.02.032
19. Kim WK, Ryu WHM, Han DW, Lim SJ, Eom JY, Kwon HS (2014) Fabrication of graphene embedded $LiFePO_4$ using a catalyst assisted self assembly method as a cathode material for high power lithium-ion batteries. ACS Appl Mater Interfaces 6:4731–4736. doi:10.1021/am405335k
20. Ding Y, Jiang Y, Xua F, Yin J, Ren H, Zhuo Q, Long Z, Zhang P (2010) Preparation of nano-structured $LiFePO_4$/graphene composites by co-precipitation method. Electrochem Commun 12:10–13. doi:10.1016/j.elecom.2009.10.023
21. Wang DY, Li H, Shi SQ, Huang XJ, Chen LQ (2005) Improving the rate performance of $LiFePO_4$ by Fe-site doping. Electrochim Acta 5:2955–2958. doi:10.1016/j.electacta.2004.11.045
22. Wang WL, Jin EM, Gu HB (2012) Electrochemical performance of lithium ion phosphate by adding graphite nanofiber for lithium ion batteries. Trans Electr Electron Mater 13:121–124. doi:10.4313/TEEM.2012.13.3.121
23. Nguyen VH, Wang WL, Jin EM, Gu HB (2013) Electrochemical characterization of $LiFePO_4$/poly(sodium 4-styrenesulfonate)-multi walled carbon nanotube composite cathode material for lithium ion batteries. J Alloy Compd 569:29–34. doi:10.1016/j.jallcom.2013.03.139
24. Nguyen HV, Jin EM, Gu HB (2012) Preparation and electrochemical properties of $LiFePO_4$-PSS composite cathode for lithium-ion batteries. Trans Electr Electron Mater 13:177–180. doi:10.4313/TEEM.2012.13.4.177
25. Culluity BD, Stock SR (2011) Element of X-ray diffraction, 3rd edn. Prentice Hall, Upper Saddle River
26. Fu ZW, Guan XF, Li LP, Li GS, Zheng J (2011) Microstructural characteristics of hydrothermally synthesized $LiFePO_4$ and relevant impacts on the electrochemical performance. Chinese J Struct Chem 30:975–986
27. He P, Zhao X, Wang YG, Cheng L, Xia YY (2008) Lithium-ion intercalation behaviour of $LiFePO_4$ in aqueous and nonaqueous electrolyte solutions. J Electrochem Soc 155:A144–A150. doi:10.1149/1.2815609
28. Rui XH, Ding N, Liu J, Li C, Chen CH (2010) Analysis of the chemical diffusion coefficient of lithium ions in $Li_3V_2(PO_4)_3$ cathode material. Electrochim Acta 55:2384–2390. doi:10.1016/j.electacta.2009.11.096
29. Franger S, Bourbon C, Le Cras F (2004) Optimized lithium iron phosphate for high-rate electrochemical applications. J Electrochem Soc 151:A1024–A1027. doi:10.1149/1.1758721
30. Sauvage F, Baudrin E, Gengembre L, Tarascon JM (2005) Effect of texture on the electrochemical properties of $LiFePO_4$ thin films. Solid State Ionics 176:1869–1876. doi:10.1016/j.ssi.2005.05.012
31. Sauvage F, Baudrin E, Morcrette M, Tarascon JM (2004) Pulsed laser deposition and electrochemical properties of $LiFePO_4$ thin films. Electrochem Solid State Lett 7:A15–A18. doi:10.1149/1.1795052
32. Delacourt C, Laffont L, Bouchet R, Wurm C, Leriche JB, Morcrette M, Tarascon JM, Masquelier C (2005) Towards the understanding of electrical limitations (electronic, ionic) in LiMPO4(M = Fe, Mn) electrode materials. J Electrochem Soc 152:A913–A921. doi:10.1149/1.1884787
33. Kanoh H, Feng Q, Miyai Y, Ooi K (1995) Kinetic properties of a Pt/Lambda-MnO_2 electrode for the electroinsertion of lithium ions in an aqueous phase. J Electrochem Soc 142:702–707. doi:10.1149/1.2048520
34. Zhao D, Feng YL, Wang YG, Xia YY (2013) Electrochemical performance comparison of $LiFePO_4$ supported by various carbon

materials. Electrochim Acta 88:632–638. doi:10.1039/C2CP24062A
35. Nguyen VH, Wang WL, Jin EM, Gu HB (2013) Impacts of different polymer binders on electrochemical properties of $LiFePO_4$ cathode. Appl Surf Sci 282:444–449. doi: 10.1016/j.apsusc.2013.05.149
36. Wang K, Cai R, Yuan T, Yu X, Ran R, Shao ZP (2009) Process investigation, electrochemical characterization and optimization of $LiFePO_4$/C composite from mechanical activation using sucrose as carbon source. Electrochim Acta 54:2861–2868. doi:10.1016/j.electacta.2008.11.012
37. Jin B, Jin EM, Park KH, Gu HB (2008) Electrochemical properties of $LiFePO_4$-multiwalled carbon nanotubes composite cathode materials for lithium polymer battery. Electrochem Commun 10:1537–1540. doi:10.1016/j.elecom.2008.08.001
38. Sun K, Dillon SJ (2011) A mechanism for the improved rate capability of cathodes by lithium phosphate surficial films. Electrochem Commun 13:200–202. doi:10.1016/j.elecom.2010.12.013